23rd ABCM International Congress of Mechanical Engineering
December 6-11, 2015, Rio de Janeiro, RJ, Brazil

INFLUENCE OF CURVATURE VARIATIONS ON THE HEAT TRANSFER IN A TRANSITIONAL BOUNDARY LAYER

Larissa Ferreira Marques
Josuel Kruppa Rogenski
Leandro Franco de Souza
Departament of Applied Mathematics and Statistics, ICMC - University of Sao Paulo, Sao Carlos, Sao Paulo, Brazil
laraposmac@gmail.com; josuelkr@gmail.com; lefraso@gmail.com

Abstract. *The centrifugal instability mechanism for boundary layers over concave surfaces is responsible for the formation of streamwise vortices known as Goertler vortices. These vortices distort both the hydrodynamic and thermal boundary layer profiles by creating two characteristic regions: the upwash region where low velocity fluid is pushed away from the wall and the downwash region, where the opposite occurs. High-order, pseudo-spectral numerical simulations are carried out to analyze the influence of the curvature variations on the hydrodynamic and thermal boundary layers. Fully concave, concave-flat and concave-convex configurations are considered. Results provide evidence that one may effectively increase heat transfer rates by changing the curvature.*

Keywords: *boundary layers, Goertler vortices, curvature variations, heat transfer, laminar-turbulent transition*

1. INTRODUCTION

The laminar-turbulent transition phenomenon has been investigated in the scientific community for over a century. Particularly, the origin of streamwise vortices in boundary layer flows and its influence in heat transfer enchancement is discussed in researches related to this area.

Different approaches related to this subject have been presented both in theorical studies (Saffmann, 1992) as well as in computational studies (Liu and Lee, 1995). According to Liu and Lee (1995), Goertler vortices generate strong distortions in the velocity profiles, modifying the main flow by pumping low momentum fluid away from the wall in what is called the upwash region, and pumping high momentum fluid close to the wall in a downwash region. The increase in the amplitude of the vortices in a non-linear development region gives rise to a mushroom-type structure, with the streamwise velocity distribution in a crosscut plane. This new velocity distribution differs from the Blasius boundary layer. Therefore a spanwise average increase in the heat transfer is observed. Moreover, there are experimental studies that compares the enhancement in heat transfer in Goertler flow with turbulent values, proving that the enhancement in heat transfer in Goertler flow can be higher than the one in turbulent flows, e.g. Peerhossaini (1987).

The search for more efficient systems to reduce energy consumption has been a challenge to heat transfer rates with minimal penalty. Fiebig (1996) to analyse the influence of longitudinal vortices on the heat transfer in boundary layer flow, concludes that these vortices are more efficient if compared with the transverse vortices for heat transfer enhancement.

More recent studies conducted by Liu (2008) show the gain in heat transfer in a flow over a slightly concave surface. Furthermore, his investigations prove that it is possible to enhance the heat transfer and that the increase in drag is not as large as the generated by winglets. Studies conducted by Momayez *et al.* (2009) show that the enhancement of heat transfer relates to the growth of Goertler vortices under the effect of centrifugal instability and secondary instabilities.

Hall (1988) and Benmalek and Saric (1994) conducted investigations related to nonlinear spatial stability computations for walls with variable concave curvature. In (Hall, 1988), disturbance quantities were expanded in Fourier series truncated in the spanwise variable z, solving the problem with a finite-difference scheme. Benmalek and Saric (1994) studied numerically the influence of variations in the curvature using the parabolized disturbance equations.

In the present paper it is studied numerically the influence of curvature variation in heat transfer enhancement, considering a boundary layer flow over wall concave followed by two different distributions of curvature. The problem is modeled through a governing system written in vorticity-velocity formulation. A simulation code was developed and implemented using a high-order, pseudo-spectral numerical simulation method. Results show that it is possible to effectively increase the heat transfer rates using a variable curvature. Furthermore, according to the results, the Prandtl number is a factor that may influence the increase of heat transfer. It is observed that independently of temperature distribution, taking $Pr = 7.07$, the heat transfer in the Goertler flow is lower than the heat transfer obtained in turbulent flow.

2. GOVERNING EQUATIONS

We consider a two-dimensional boundary layer flow over a concave surface with curvature variation. For stability analysis, we assume that vorticity and velocity components are composed of a baseflow and a disturbance

$$\widetilde{p} = p_b + p,$$

where $\widetilde{p} = \left\{\widetilde{u}, \widetilde{v}, \widetilde{w}, \widetilde{\omega}_x, \widetilde{\omega}_y, \widetilde{\omega}_z, \widetilde{\theta}\right\}$ corresponds to the total amounts of velocity, vorticity and temperature components, p_b denotes the baseflow and the disturbance is represented by p. In this formulation the linear and nonlinear terms can be isolated. This facilitates stability analysis of any baseflow.

Defining the vorticity as the negative curl of the velocity vector, and using the fact that both, the velocity and the vorticity fields are solenoidal, we obtain the following dimensionless vorticity transport equations in the streamwise (x), wall-normal (y) and spanwise (z) directions (Souza *et al.*, 2004) :

$$\frac{\partial \omega_x}{\partial t} + \frac{\partial a}{\partial y} - \frac{\partial b}{\partial z} + \frac{Go^2}{\sqrt{Re}}\frac{\partial d}{\partial z} = \frac{1}{Re}\nabla^2 \omega_x, \tag{1}$$

$$\frac{\partial \omega_y}{\partial t} + \frac{\partial c}{\partial z} - \frac{\partial a}{\partial x} = \frac{1}{Re}\nabla^2 \omega_y, \tag{2}$$

$$\frac{\partial \omega_z}{\partial t} + \frac{\partial b}{\partial x} - \frac{\partial c}{\partial y} - \frac{\partial}{\partial x}\frac{Go^2 d}{\sqrt{Re}} = \frac{1}{Re}\nabla^2 \omega_z. \tag{3}$$

The heat transfer transport equation adopted in the present study is:

$$\frac{\partial \theta}{\partial t} + \frac{\partial e}{\partial x} + \frac{\partial f}{\partial y} + \frac{\partial g}{\partial z} = \frac{1}{Re\, Pr}\nabla^2 \theta, \tag{4}$$

where $\nabla^2 = \left(\frac{\partial^2}{\partial x^2} + \frac{\partial^2}{\partial y^2} + \frac{\partial^2}{\partial z^2}\right)$ denotes the Laplace operator, $\theta = (T - T_0)/(T_\infty - T_0)$ is the nondimensional temperature, being T the dimensional temperature, T_∞ and T_0 the temperature values outside from the thermal boundary layer and at the wall, respectively.

The Eqs. (1) – (3) and (4) were dimensionless using the nondimensional parameters Re, Go and Pr, known as Reynolds, Goertler and Prandtl numbers, defined respectively by

$$Re = \frac{U_\infty^* L^*}{\nu^*}, \;\; Go = Re^{\frac{1}{4}}\sqrt{\frac{L^*}{R^*}}, \;\; Pr = \frac{\nu^*}{\alpha^*},$$

where ν^* denotes the kinematic viscosity, L^* is a plate characteristic length and the free stream velocity is denoted by U_∞^*. The curvature radius of the concave surface is represented by R^* and α^* is the thermal diffusivity of the fluid.

The nonlinear components a, b, c, d, e, f and g shown in Eqs. (1) – (3) and (4) are defined by

$$\begin{aligned}
a &= \omega_x(v_b + v) - \omega_y(u_b + u),\\
b &= \omega_{zb} u + \omega_z(u_b + u) - \omega_x w,\\
c &= (w_b + w)\omega_y - (v_b + v)\omega_z - \omega_{zb} v,\\
d &= 2u_b u + u^2,\\
e &= \theta(u_b + u) + \theta_b u,\\
f &= \theta(v_b + v) + v\theta_b,\\
g &= w_b(\theta_b + \theta).
\end{aligned}$$

The continuity equation is given by

$$\frac{\partial u}{\partial x} + \frac{\partial v}{\partial y} + \frac{\partial w}{\partial z} = 0. \tag{5}$$

From the definition of vorticity and the mass conservation equation, we obtain Poisson equations for each velocity component:

$$\frac{\partial^2 u}{\partial x^2} + \frac{\partial^2 u}{\partial z^2} = -\frac{\partial \omega_y}{\partial z} - \frac{\partial^2 v}{\partial x \partial y}, \tag{6}$$

$$\frac{\partial^2 v}{\partial x^2} + \frac{\partial^2 v}{\partial y^2} + \frac{\partial^2 v}{\partial z^2} = -\frac{\partial \omega_z}{\partial x} + \frac{\partial \omega_x}{\partial z}, \tag{7}$$

$$\frac{\partial^2 w}{\partial x^2} + \frac{\partial^2 w}{\partial z^2} = \frac{\partial \omega_y}{\partial x} - \frac{\partial^2 v}{\partial y \partial z}. \tag{8}$$

Therefore, Eqs. (1) – (3), (4) and (5), (6) – (8) close the system of equations for disturbances. Mean-flow values are calculated considering the Blasius boundary layer approximation (Schlichting, 1979).

3. NUMERICAL METHOD

The numerical method used to solve the system of equations for mean-flow presented in the Section 2. is based in high order compact finite difference approximations for the discretization of the streamwise and wall normal spatial derivatives (Petri *et al.*, 2015). In the spanwise direction a spectral method based on Fast Fourier transformation was adopted. The time integration was carried out by a classical fourth order Runge-Kutta scheme. A buffer-domain technique was considered to avoid reflection of disturbances at the boundaries. The computational domain is illustrated in Fig. 1.

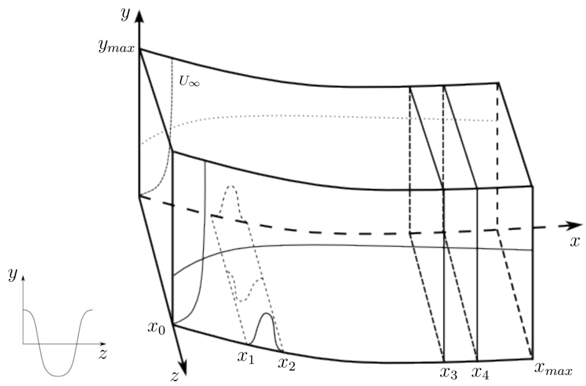

Figure 1. Computational domain.

Assuming that there is periodicity in the spanwise direction of the flow we adopted a spectral method. Each total amounts of velocity and vorticity components denoted by $\widetilde{p}$, can be written as a linear combination of the $k+1$ spanwise Fourier modes

$$p(x,y,z,t) = \sum_{k=0}^{K} p_k(x,y,t) e^{-\iota k \beta z}, \tag{9}$$

where ι is the imaginary unit, β denotes the spanwise wavenumber and it is given by

$$\beta = \frac{2\pi}{\lambda_z},$$

and λ_z is the dimensionless wavelength in the spanwise direction.

Substituting the Fourier transforms given by Eq. (9) in the Eqs. (1) – (3), (4) and (6) – (8), one obtains the governing equations in the Fourier space:

$$\frac{\partial \omega_{x_k}}{\partial t} + \frac{\partial a_k}{\partial y} + \iota k \beta b_k - \iota k \beta d_k \frac{Go^2}{\sqrt{Re}} = \frac{1}{Re} \nabla_k^2 \omega_{x_k}, \tag{10}$$

$$\frac{\partial \omega_{y_k}}{\partial t} - \iota k \beta c_k - \frac{\partial a_k}{\partial x} = \frac{1}{Re} \nabla_k^2 \omega_{y_k}, \tag{11}$$

$$\frac{\partial \omega_{z_k}}{\partial t} + \frac{\partial b_k}{\partial x} - \frac{\partial c_k}{\partial y} - \frac{\partial d_k}{\partial x} \frac{Go^2}{\sqrt{Re}} = \frac{1}{Re} \nabla_k^2 \omega_{z_k}, \tag{12}$$

$$\frac{\partial^2 u_k}{\partial x^2} - k^2 \beta^2 u_k = -\iota k \beta \omega_{y_k} - \frac{\partial^2 v_k}{\partial x \partial y}, \tag{13}$$

$$\frac{\partial^2 v_k}{\partial x^2} + \frac{\partial^2 v_k}{\partial y^2} - k^2 \beta^2 v_k = -\frac{\partial \omega_{z_k}}{\partial x} - \iota \beta \omega_{x_k}, \tag{14}$$

$$\frac{\partial^2 w_k}{\partial x^2} - k^2 \beta^2 w_k = \frac{\partial \omega_{y_k}}{\partial x} + \iota k \beta \frac{\partial v_k}{\partial y}, \tag{15}$$

$$\frac{\partial \theta_k}{\partial t} + \frac{\partial e_k}{\partial x} + \frac{\partial f_k}{\partial y} + \iota k \beta g = \frac{1}{Re\, Pr} \nabla_k^2 \theta_k, \tag{16}$$

where $\nabla_k^2 = \left(\frac{\partial^2}{\partial x^2} + \frac{\partial^2}{\partial y^2} - k^2 \beta^2 \right)$.

The nonlinear coupled system of equations given by Eqs. (10) – (16) is solved numerically in the domain shown schematically in Fig. 1. The inflow boundary is represented by $x = x_0$ and the outflow boundary, $x = x_{max}$. Disturbances are introduced into the flow field using spanwise suction and blowing of mass at the wall in a disturbance strip at the wall located in the region between points x_1 and x_2. In order to avoid wave reflections at the outflow boundary we implemented in the region located between x_3 and x_4 a buffer domain technique (Kloker *et al.*, 1993). In these simulations we assume the mean flow state as a Blasius boundary layer solution and for the thermal boundary layer, the standard similarity solution obtained by Pohlhausen formula was used.

For the discretization of the time derivatives in the vorticity transport equations it was used a classical 4^{th} order Runge-Kutta integration scheme (Ferziger and Peric, 1997). The calculation of spatial derivatives were done using a high order compact finite difference-schemes (Souza *et al.*, 2005). The v-Poisson equation, defined in Eq. (14), was solved using a multigrid Full Approximation Scheme (FAS) (Stüben and Trottenberg, 1981). For the implementation we adopted a V-cycle working with four levels. The solution will converge, ie, the steady state is reached when the maximum difference between the $k = 1$ spanwise vorticity component is smaller than a given considerably small parameter in two consecutive time steps.

3.1 The boundary conditions

The following boundary conditions were adopted to complete the governing equations:

- In $y = 0$, ie., at the wall, we impose a no-slip condition for the streamwise u_k and the spanwise w_k velocity components.
- In the suction and blowing strip region, we specify the wall-normal velocity component at the wall v_k and away from the disturbance generator this velocity component was set to zero.
- The function used for the wall-normal velocity v_1 at the disturbance generator is imposed to have a $\sin^3$ shape.
- In $x = x_0$, the velocity, the vorticity components and the temperature are zero. In the same way, to $x = x_{max}$, the second derivatives with respect to the streamwise direction of the velocity and vorticity components are set to zero.
- At the upper boundary ($y = y_{max}$) the flow is considered nonrotational. We defined the wall-normal velocity component at $y = y_{max}$ according to the condition: $\left.\frac{\partial v_k}{\partial y}\right|_{x,y_{max},t} = 0$. In addition, at the wall, the condition $\frac{\partial v_k}{\partial y} = 0$ was imposed in the solution of the u_k velocity Poisson equation (Eq.13).
- The expressions used for calculated the vorticity components at the wall are:

$$\begin{aligned}
\frac{\partial^2 \omega_{x_k}}{\partial x^2} - k^2\beta^2\omega_{x_k} &= -\frac{\partial^2 \omega_{y_k}}{\partial x \partial y} - \beta\nabla_k^2 v_k, \\
\omega_{y_k} &= 0, \\
\frac{\partial \omega_{z_k}}{\partial x} &= \iota k\beta\omega_{x_k} - \nabla_k^2 v_k.
\end{aligned}$$

- The boundary conditions for the temperature were:
  - (i) inflow – $\theta = 0$;
  - (ii) outflow – $\theta = 0$, since the same buffer domain for the vorticity was also applied for the temperature;
  - (iii) wall – $\theta = 0$;
  - (iv) upper boundary – the values were obtained from the heat transfer transport equation.

4. RESULTS

The nonlinear simulations were made adopting the same physical parameters of the classical experiments of Swearingen and Blackwelder (1987). We consider the radius of the concave surface $R^* = 3.2\ m$, the free stream velocity $U_\infty^* = 5\ ms^{-1}$, the kinematic viscosity $\nu^* = 1,5 \times 10^{-5}\ m^2s^{-1}$, the time step $dt = 4 \times 10^{-3}$, the number of points in the x and y directions 537 and 185, respectively. The distance between two consecutive points in the x and y directions are $dx = 4 \times 10^{-2}$ and $dy = 8.5 \times 10^{-4}$. The disturbances were introduced in the region $1.76 \leq x \leq 2.36$, with an amplitude of $A = 5 \times 10^{-3}$, whereas two different spanwise wavelengths, $\lambda_z^* = 1.8 \times 10^{-2}\ m$ for the case of constant curvature and $\lambda_z^* = 1.57 \times 10^{-2}\ m$ for the other curvature distributions. In the z direction 11 Fourier modes were used with 32 points in the physical space.

We adopted as a metric for analyze the disturbance evolution the energy of each Fourier mode, given by

$$E_k(x) = \int_0^\infty |u_k|^2\, dy.$$

For analysis of heat transfer we verify the evolution of the spanwise–average Stanton number in the streamwise direction, where this nondimensional parameter is defined as

$$St_x = \frac{Nu_x}{PrRe_x}, \text{ with } Nu_x = \left.\frac{\partial T}{\partial y}\right|_{wall} \frac{L}{T_e - T_w},$$

where Nu_x denotes the Nusselt number.

For each case of curvature variation three Prandtl numbers were analyzed: $Pr = 0.72$, $Pr = 1.0$ and $Pr = 7.07$. Thus allow the investigation of the behavior of heat transfer rate with different fluid properties.

4.1 Constant curvature wall

The first distribution of curvature to be analyzed is a classic case where the curvature is fully concave, i.e., $\frac{k}{k_0} = 1$, where k_0 is the curvature at the position $x = 1$ and k is the curvature at a x position.

Figure 2 shows the streamwise evolution of the amplitudes $E_k, 0 \leq k \leq 10$, of the streamwise vortices. The region defined by $5 \leq x \leq 9$ $(1.6 \times 10^5 \leq Re_x \leq 3 \times 10^5)$ is characterized by linear growth of the Goertler vortices. In the saturation region, $x \geq 9.5$ $(Re_x \geq 3.1 \times 10^5)$, it is noted that the difference between the amplitude of consecutive modes are almost constant. We can also observe qualitative agreement between the data of the first four modes obtained in this study with the data presented by Benmalek and Saric (1994).

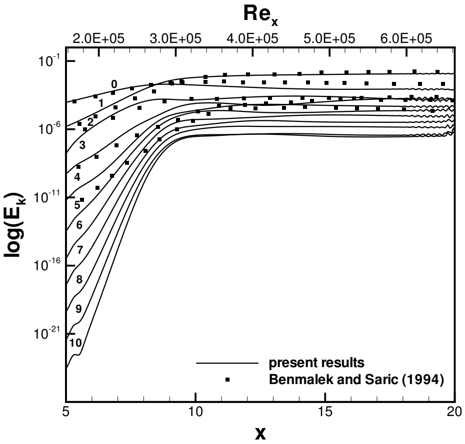

Figure 2. Energy distribution for each Fourier mode in the streamwise direction for $\lambda_z = 1.8 \times 10^{-1}$. Constant curvature wall case.

The streamwise evolution of the average Stanton number, considering three different Prandtl numbers, is shown in Fig. 3.

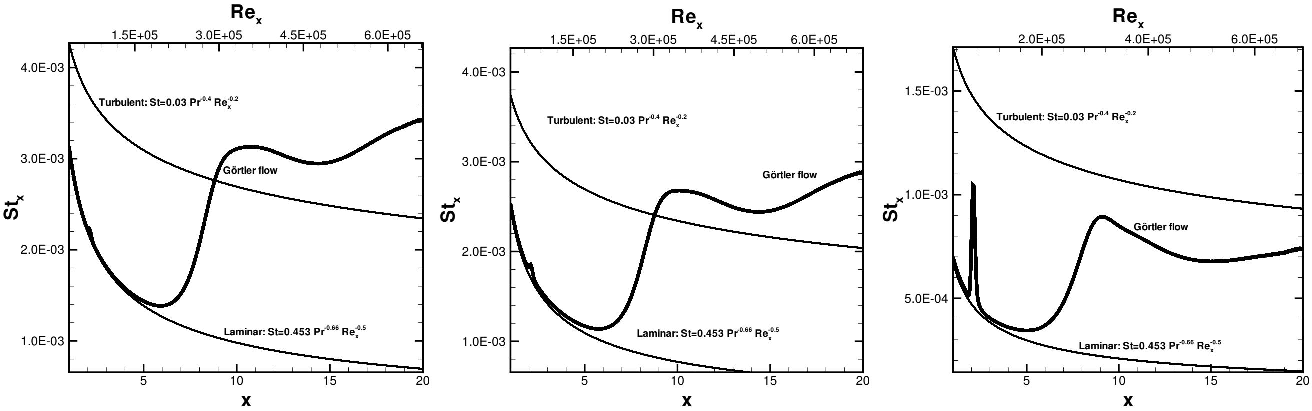

(a) $Pr = 0.72$ (b) $Pr = 1.0$ (c) $Pr = 7.07$

Figure 3. Streamwise evolution of the spanwise-averaged Stanton number for $\lambda_z = 0.18$. Transitional results are compared with laminar and turbulent boundary layer theoretical Stanton functions (Schlichting, 1979).

Analyzing the three cases presented in Fig. 3 we can see that in the region until $Re_x \sim 1.3 \times 10^5$ $(x \sim 3.8)$ the spanwise-averaged Stanton number for the Goertler flow is similar to laminar flow. The region $2 \times 10^5 \leq Re_x \leq 3 \times 10^5$ $(6.5 \leq x \leq 9)$ is characterized by intensification of rate of heat transfer caused by the Goertler flow.

In the first case, where $Pr = 0.72$, at the Re_x around 6.38×10^5 $(x \sim 19)$, the Stanton number reaches higher values than the turbulent ones. In this position the Stanton number with Goertler flow is 391% and 46% higher than laminar and turbulent values, respectively. On the other hand, to $Pr = 7.07$, the Stanton number for the Goertler flow does not reach the Stanton number obtained in turbulent flow by the fact that the thermal boundary layer is much thicker than the hydrodynamic boundary layer, therefore the influence of Goertler vortices is smaller.

4.2 Concave/convex wall

For this analysis, we take a concave circular arc attached to a convex circular arc of the same radius $\frac{1}{k_0}$ by a section with continuously variable curvature. The function representing the curvature distribution is given by $\frac{k}{k_0} = -\tanh[3(x-8)]$.

Figure 4 shows energy distribution in the streamwise direction for the steady modes from 1 to 10, and also the mean flow represented by mode 0. Through the fundamental mode $(k = 1)$ we can see the highest energy level in the linear region. Between the x equal 5 until 8 $(1.6 \times 10^5 \leq Re_x \leq 2.6 \times 10^5)$ one can observed the linear growth of all modes. One may note that in this case there is no saturation of the vortices. The results of Benmalek and Saric (1994) are also presented in the Fig. 4, showing a good agreement with present results.

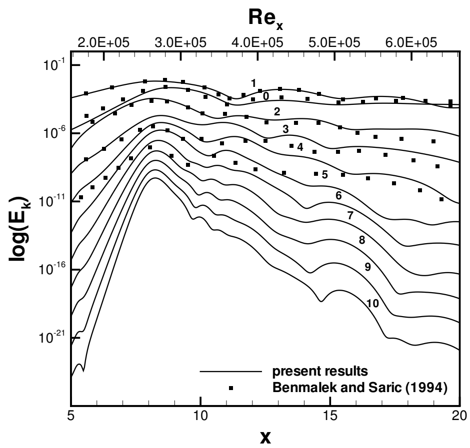

Figure 4. Energy distribution for each Fourier mode in the streamwise direction for $\lambda_z = 1.57 \times 10^{-1}$. Concave/convex curvature wall case.

As in the previous case, a heat transfer analysis was carried with three different Prandtl numbers. The results are illustrated in Fig. 5.

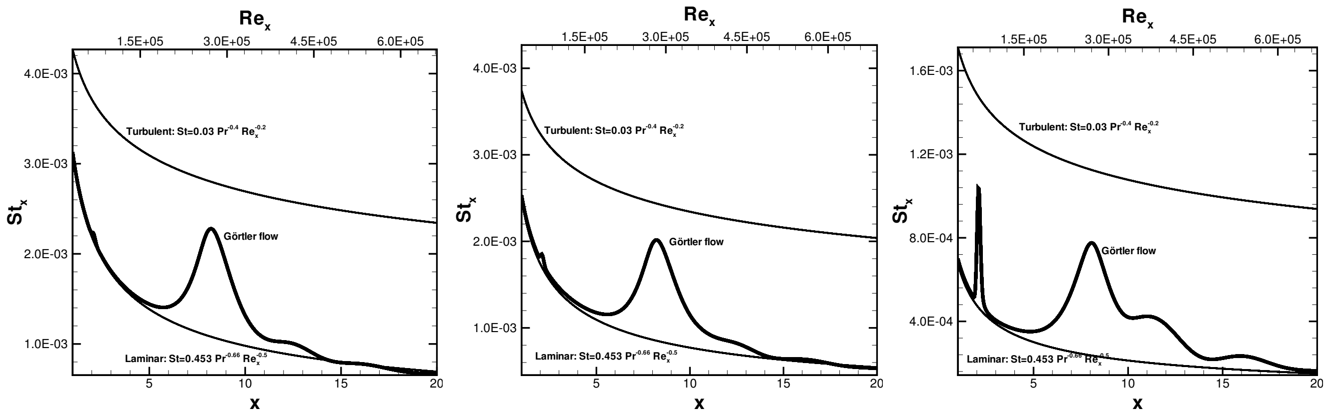

(a) $Pr = 0.72$ (b) $Pr = 1.0$ (c) $Pr = 7.07$

Figure 5. Streamwise evolution of the spanwise-averaged Stanton number for $\lambda_z = 0.157$. Transitional results are compared with laminar and turbulent boundary layer theoretical Stanton functions (Schlichting, 1979).

At the beginning when the vortices are in the linear development region, the Stanton curve for the Goertler flow coincides with the Stanton curve for the laminar flow. For all the cases presented, the heat transfer from the transitional flow does not reach the heat transfer turbulent values. Also we observed that the Stanton curve for Goertler flow tends to resume the same behavior of Stanton curve for laminar flow. Taking the case where $Pr = 1.0$, the highest value of the Stanton number is achieved in the transitional flow was at $Re_x = 2.7 \times 10^5$ $(x = 8.2)$, where the Stanton number with Goertler flow is 132% higher and 22% lower than laminar and turbulent values, respectively.

4.3 Concave/flat wall

For the last case analyzed, we consider a wall consisting of a concave section attached to a flat section by a section with continuous variable curvature. The curvature distribution is taken as $\frac{k}{k_0} = \frac{1}{2} - \frac{1}{2}\tanh[3(x - 10.24)]$.

In Fig. 6 the effect of the streamwise vortices can be seen from the distribution of the amplitudes E_k, $0 \leq k \leq 10$. In the concave section, $x \leq 10.24$ ($Re_x \leq 3.5 \times 10^5$), the amplitude E_k of the vortices for all Fourier modes increase.

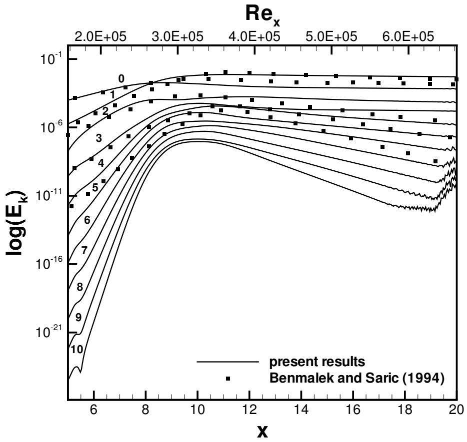

Figure 6. Energy distribution for each Fourier mode in the streamwise direction for $\lambda_z = 1.57 \times 10^{-1}$. Concave/zero curvature wall case.

The same analysis of the Stanton number distribution in the streamwise direction was carried out, and the result is shown in Fig. 7.

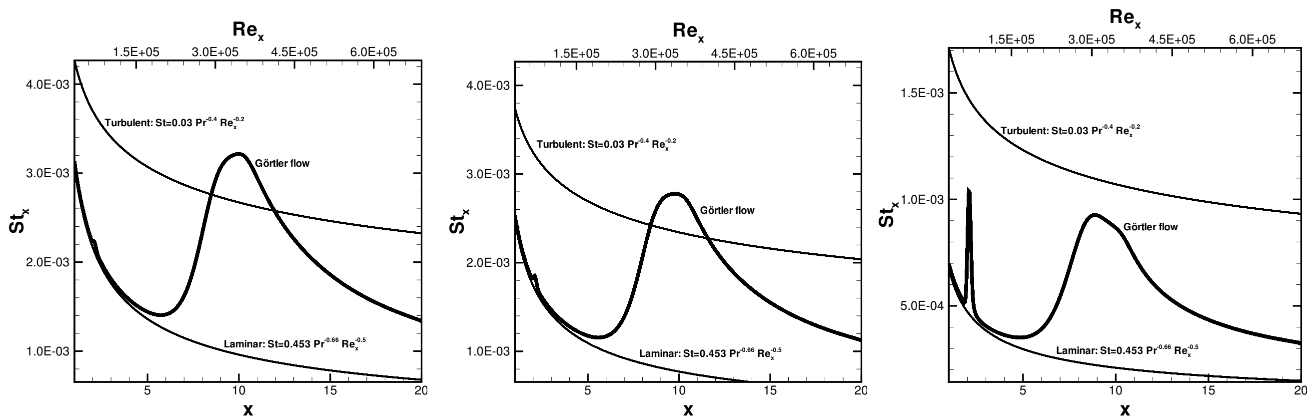

(a) $Pr = 0.72$ (b) $Pr = 1.0$ (c) $Pr = 7.07$

Figure 7. Streamwise evolution of the spanwise-averaged Stanton number for $\lambda_z = 0.157$. Transitional results are compared with laminar and turbulent boundary layer theoretical Stanton functions (Schlichting, 1979).

For the cases shown in the Fig.7, items (a) and (b), the Stanton number with Goertler flow exceeds the number of Stanton with turbulent flow in the area $2.9 \times 10^5 \leq Re_x \leq 4.1 \times 10^5$ ($8.5 \leq x \leq 12$). For $Pr = 0.72$, at $Re_x = 3.5 \times 10^5$ ($x = 10$) the Stanton number with Goertler flow reaches 226% and 19% higher than laminar and turbulent values, respectively. Taking $Pr = 1.0$. The Stanton number with transitional flow has a peak at $Re = 3.4 \times 10^5$ ($x = 9.7$), where it is 250% and 79% higher than laminar and turbulent values.

5. CONCLUSIONS

Heat transfer enhancement investigations, considering a boundary layer flow over wall with curvature variation have been numerically studied using a high-order numerical simulation code. The results in this study show that the case of concave/convex curvature has effects of stability on Goertler vortices generated by the concave curvature. Thus there is evidence that the convex curvature can be most useful for the control of a laminar flow. Considering the other curvature distributions, it was observed that the steady Goertler flow can increase the heat transfer rates to values higher than the turbulent ones. Furthermore, the results show that for $Pr = 7.07$, the Goertler flow does not reach the Stanton number obtained in turbulent flow in any of the cases analyzed. This is justified due to the fact that the thermal boundary layer is thicker than the hydrodynamic boundary layer, so the influence of Goertler vortices is smaller.

6. REFERENCES

Benmalek, A. and Saric, W.S., 1994. "Effects of Curvature Variation on the Nonlinear Evolution of Goertler Vortices". *Physics of Fluids*, Vol. 6, pp. 3353–3367.

Ferziger, J.H. and Peric, M., 1997. *Computational Methods for Fluid Dynamics*. Springer-Verlag Berlin Heidelberg New York.

Fiebig, M., 1996. "Vortices and heat transfer". *Z. Angew. Math. Mech.*, Vol. 366, pp. 2699–2716.

Hall, P., 1988. "The nonlinear development of Gortler vortices in growing boundary layers". *I. Fluid Mech.*, pp. 193–243.

Kloker, M., Konzelmann, U. and Fasel, H., 1993. "Outflow boundary conditions for spatial Navier-Stokes simulations in transition boundary layers". *AIAA Journal*, Vol. 31, pp. 620–628.

Liu, J.T.C., 2008. "Nonlinear instability of developing streamwise vortices with applications to boundary layer heat transfer intensification through an extended Reynolds analogy". *Philolsofical Transactions of the Royal Society*, Vol. 366, pp. 2699–2716.

Liu, J.T.C. and Lee, K., 1995. "Heat transfer in a strongly spatially developing longitudinal vorticity system". *Physics of Fluids*, Vol. 7, pp. 559–599.

Momayez, L., Dupont, P., Delacourt, G., Lottin, O. and Peershossaini, H., 2009. "Genetic algorithm based correlations for heat transfer calculation on concave surfaces". *Applied Thermal Engineering*, Vol. 29, pp. 3476–3481.

Peerhossaini, H., 1987. *L'Instabilite d'une couche limite sur une paroi concave: les tourbilons de Goertler*. Ph.D. thesis, Univ. Pierre et Marie Curie.

Petri, L., Sartori, P., Rogenski, J.K. and Souza, L.F., 2015. "Verification and validation of a Direct Numerical Simulation code". *Computer methods in applied mechanics and engineering*, Vol. 291, pp. 266–279.

Saffmann, P.G., 1992. *Vortex Dynamics*. Cambridge University Press.

Schlichting, H., 1979. *Boundary-Layer Theory*. McGraw-Hill, IncH.

Souza, L.F., Mendonça, M.T., de Medeiros, M.A.F. and Kloker, M., 2004. "Seeding of Görtler vortices through a suction and blowing strip". *Journal of the Brazilian Society of Mechanical Sciences*, Vol. XXVI, pp. 269–279.

Souza, L.F., Mendonça, M.T. and Medeiros, M.A.F., 2005. "The advantages of using high-order finite differences schemes in laminar-turbulent transition studies". *International Journal for Numerical Methods in Fluids*, Vol. 48, pp. 565–592.

Stüben, K. and Trottenberg, U., 1981. *Nonlinear multigrid methods, the full approximation scheme*, Köln-Porz, chapter 5, pp. 58–71. Lecture Notes in Mathematics.

Swearingen, J.D. and Blackwelder, R.F., 1987. "The growth and breakdown of streamwise vortices in the presence of a wall". *J. Fluid Mech.*, Vol. 182, pp. 255–290.

7. RESPONSIBILITY NOTICE

The authors are the only responsible for the printed material included in this paper.